Microchim Acta (2017) 184:3729–3737
DOI 10.1007/s00604-017-2373-2

ORIGINAL PAPER

Boronate-affinity based magnetic molecularly imprinted nanoparticles for the efficient extraction of the model glycoprotein horseradish peroxidase

Xiao-Yu Sun[1,2] · **Run-Tian Ma**[1] · **Juan Chen**[1] · **Yan-Ping Shi**[1]

Received: 14 March 2017 / Accepted: 12 June 2017 / Published online: 5 July 2017

Abstract Magnetic molecularly imprinted nanoparticles (MMIPs) with improved dispersity and an increased number of adsorption sites are described. Uniform silica layers were first deposited on the surface of Fe_3O_4 nanoparticles (Fe_3O_4 NPs) in order to improve the dispersity of magnetic nanoparticles. Then, 4-formylphenylboronic acid (FPBA) as functional monomer was immobilized on the magnetic carriers to improve the efficiency of template eluting and rebinding. A thin layer of polyaniline imprinted with horseradish peroxidase (HRP) as a model glycoprotein was then placed on the magnetic nanoparticles to enhance the dispersity of the resultant MMIPs. These exhibit high adsorption capacity (62 mg g^{-1}), a satisfactory imprinting factor (3.78) and short adsorption equilibrium time (40 min) toward HRP, and the limit of detection is 18.7 μg L^{-1}. This kind of MMIPs, therefore, is deemed being a useful tool for extracting low-abundance glycoproteins from even complex samples.

Electronic supplementary material The online version of this article (doi:10.1007/s00604-017-2373-2) contains supplementary material, which is available to authorized users.

✉ Juan Chen
chenjuan@licp.cas.cn

✉ Yan-Ping Shi
shiyp@licp.cas.cn

[1] Key Laboratory of Chemistry of Northwestern Plant Resources and Key Laboratory for Natural Medicine of Gansu Province, Lanzhou Institute of Chemical Physics, Chinese Academy of Sciences, Lanzhou 730000, China

[2] University of Chinese Academy of Sciences, Chinese Academy of Sciences, Beijing 100049, People's Republic of China

Keywords Fe_3O_4 nanoparticles · MIPs · Improved dispersity · Thin imprinted layer · Surface imprinting

Introduction

Glycoproteins play an important role in biological process. Numerous studies have proven that the expression of various glycoproteins is closely related to the occurrence of diverse diseases, such as diabetes, cancer, neurodegenerative diseases and cardiovascular disease [1–6]. An overview on the nanomaterials-based methods reported within five years for the extraction of glycoproteins is presented in Table S1. Considerable efforts has been paid to extract low-abundance glycoproteins from complex samples, such as hydrophilic interaction chromatography [7], hydrazine chemistry [8], and boronate-affinity chromatography [9]. Although the above materials have alleviated the difficulty but they cannot extract the targets specifically. For example, boronate-affinity chromatography, lacking of specific recognition ability, tends to extract an important class of compounds as long as compounds containing cis-diols [10]. Therefore, additional method with specific recognition capability for the efficient extraction of one kind of low-abundance glycoprotein from complex samples is still urgently needed [11].

Molecularly imprinted polymers (MIPs), containing specific adsorption sites complementary in size, shape and functional groups to the template, have widely application potential in the field of specific extraction of template from complex samples [12–16]. Despite the attractive properties of molecular imprinting, the imprinting of macromolecular still be hindered greatly especially protein due to flexible conformation, large molecular size, and poor mass transfer [17–19]. Core-shelled surface molecular imprinting by reducing mass transfer routs, increasing affinity capacity and efficiently eluting template

well solved the difficulty of imprinting macromolecular, which attempts to generate adsorption sites on the surface of different materials [20]. Among them, magnetic molecularly imprinted nanoparticles (MMIPs) building adsorption sites on the surface of Fe_3O_4 nanoparticles (Fe_3O_4 NPs) have become the efficient platform for the extraction of proteins from complex samples. They have the properties of large surface-to-volume ratio, better sites accessibility and convenient separation [21–23]. However, the magnetism of Fe_3O_4 NPs and the thick imprinted layer which in company tend to wrap many MMIPs together, leading to the seriously aggregation of the resultant MMIPs [24, 25]. In this way, the number of the adsorption sites was decreased. On the other hand, the long mass transfer route resulted by the thick imprinted layer not only prolonged the adsorption time but also increase the elution and adsorption difficulties of the templates. Therefore, proper functional monomer to relieve the adsorption and elution difficulties, and thin imprinted layer to shorten the mass transfer route of template, are urgently needed to improve the conventional MMIPs.

In this work, a method for preparing MMIPs with improved dispersity via surface modification of Fe_3O_4 nanoparticles and regulating the thickness of the imprinted layer was developed. Solvothermal method was adopted to prepare Fe_3O_4 NPs and then uniform silica layers were coated on the surface of Fe_3O_4 nanoparticles to get core-shelled $Fe_3O_4@SiO_2$ NPs by sol-gel method. $Fe_3O_4@SiO_2$ NPs not only enhance the dispersity of magnetic nanoparticles but also enable magnetic nanoparticles easy to be modified with FPBA via forming covalent bound. After horseradish peroxidase (HRP) as the model glycoprotein was reversible fixed on the boronic acid-functionalized $Fe_3O_4@SiO_2$ NPs [26], the thin imprinted layers of polyaniline were formed by controlling the polymerization time. Through optimizing the polymerization time of aniline, imprinted layer with proper thickness was generated on the surface of magnetic nanoparticles. Therefore, the resultant MMIPs with improved dispersity and excellent extraction efficiency toward HRP were achieved.

Experimental

Materials and reagents

All chemicals and reagents were used without further purification. Ferric chloride ($FeCl_3 \cdot 6H_2O$), anhydrous sodium acetate (NaAc), ammonium persulfate, sodium dihydrogen phosphate (NaH_2PO_4) and disodium phosphate (Na_2HPO_4) were obtained from Sinopharm Chemical Reagent Co., Ltd. (Beijing, China, www.crc-bj.com/). Tetraethyl orthosilicate (TEOS) was purchased from Tianjin Fuyu Fine Chemical Co., Ltd. (Tianjin, China, https://fuyuhuagong.cn.china.cn/). Hydrochloric acid (HCl) and aqueous ammonia ($NH_3 \cdot H_2O$) were provided by Xilong Scientific Co., Ltd. (Guangdong, China, http://www.xlhg.com/). Aniline, 4-Formylphenylboronic acid (FPBA) and sodium cyanoborohydride ($NaBH_3CN$) were all purchased from J&K Scientific (Beijing, China, http://www.jkchemical.com/). 3-aminopropyltriethoxysilane (APTES) was obtained from Aladdin industrial corporation (Shanghai, China, http://www.aladdin-e.com/). Polyethylene glycol (PEG-6000), anhydrous methanol, anhydrous ethanol, ethylene glycol (EG), acetic acid and acetonitrile were all purchased from Rionlon Bohua (Tianjin) Pharmaceutical & Chemical Co., Ltd. (Tianjin, China, http://www.rionlon.com/). Fetal bovine serum (FBS) was bought from Zhejiang Hangzhou Bio-Techonology Co., Ltd. (Zhejiang, China, http://www.hzsjq.com). Horseradish peroxidase (HRP), ovalbumin (OVA) and bovine serum (BSA) were purchased from Shanghai Ryon Biological Technology Co., Ltd. (Shanghai, China, http://www.ryon-sh.com/).

Instruments

The UV-vis adsorption spectra of the samples were recorded using a Perkin Elmer ultraviolet-visible spectrophotometer (USA) with a 1 cm path length quartz cuvette. The morphologies of the magnetic nanoparticles were examined by transmission electron microscopy (TEM) (FEITECNAI G2TF20, USA). The average hydrodynamic diameter of nanoparticles was detected using nanoparticle size and potential analyzer (Malvern, ZEN 3600, UK). Nicolet Nexus 870 FT-IR spectrometer was used to identify the presence of certain functional groups on the magnetic nanoparticles. X-ray photoelectron spectroscopy (XPS) analysis was carried out on an ESCALAB 250Xi X-ray photoelectron spectrometer (Thermo Fisher scientific, United States). The magnetic properties of the nanoparticles were investigated at room temperature by measuring the magnetization curve via vibrating sample magnetometer (VSM) (Lakeshore 7304, USA).

Preparation of MMIPs

Solvothermal method reported previously was adopted to prepare Fe_3O_4 NPs [27]. Briefly, $FeCl_3 \cdot 6H_2O$ (1.35 g) were dispersed into EG (40 mL) to form a clear yellow solution. NaAc (3.6 g) and PEG-6000 (1.0 g) were subsequently added into the above solution under magnetic stirring. After that, vigorous stirring was kept for 30 min. Then the solution was removed into a Teflon-lined stainless-steel autoclave and kept at 200 °C for 24 h. when the reaction was completed, the product was washed with ultrapure water for several times and then dried at 60 °C for 12 h in vacuum oven.

Sol-gel method was adopted to synthesize core-shelled Fe_3O_4@SiO_2 NPs [28]. Firstly, the prepared Fe_3O_4 NPs (0.1 g) were dispersed into 0.1 M HCl solution (50 mL) with ultrasound for 30 min, and then washed with ultrapure water for several times until the washing solution was neutral. Afterwards, the nanoparticles were dispersed into the mixture of anhydrous ethanol (60 mL) and ultrapure water (20 mL) under stirring, followed by adding aqueous ammonium (1 mL) and TEOS (400 μL) drop by drop. After reacting for 24 h, the resultant products were washed with ultrapure water for several times and then dried at 60 °C for 12 h in vacuum oven.

Fe_3O_4@SiO_2 NPs (0.1 g) were dispersed into 0.1 M HCl solution (50 mL) with ultrasound for 30 min, and washed with ultrapure water for several times until the washing solution is neutral, and then dispersed into anhydrous methanol (40 mL). Subsequently, APTES (800 μL) was added into the dispersion and the mixture was refluxed at 65 °C for 24 h. The APTES modified Fe_3O_4@SiO2 NPs (Fe_3O_4@SiO_2-APTES NPs) were washed with anhydrous methanol for several times and dried at 60 °C for 12 h in vacuum oven.

The Fe_3O_4@SiO_2-APTES NPs (100 mg) were dispersed into anhydrous methanol (30 mL), followed by the successive addition of FPBA (250 mg) and $NaCNBH_4$ (300 mg) to synthesis FPBA functionalized Fe_3O_4@SiO_2 NPs (Fe_3O_4@SiO_2-FPBA NPs) [29]. The reaction was allowed to proceed under reflux for 24 h. The prepared Fe_3O_4@SiO_2-FPBA NPs were washed with anhydrous methanol for several times and then placed into vacuum oven for 12 h at 60 °C.

HRP (15 mg) were added into the dispersion of Fe_3O_4@SiO_2-FPBA NPs (60 mg) in 200 mM phosphate buffer (PB, pH 8.5, 30 mL) and the dispersion was stirred at 25 °C for 12 h. The resultant magnetic nanoparticles immobilized with HRP were washed with PB (pH 8.5, 200 mM) for several times and dried in air at room temperature. The dried nanoparticles (30 mg) were dispersed into PB (pH 8.5, 200 mM, 25 mL), then aniline (180 μL) and amonium persulfate (120 mg) were successively added into the above solution under ultrasound. Subsequently, the mixture was stirred at room temperature for 30 min. The resultant polymers were washed with 5% acetic acid aqueous solution containing 30% acetonitrile under ultrasound to remove HRP for several times until the washing solution showed no adsorption at 398 nm detected by UV-Vis spectrophotometer and then dried in air at room temperature. The same way was adopted without addition of HRP to prepare non-imprinted magnetic nanoparticles (MNIPs). The complete preparation synthesis procesure can be observed from Fig. 1.

Isothermal binding study of MMIPs

To investigate the adsorption capacity of the prepared materials, MMIPs or MNIPs were added to HRP solutions prepared in PB (pH 8.5, 200 mM) with various concentrations from 0.05 to 0.5 mg mL^{-1}. The mixtures were allowed to be incubated at 25 °C for 1 h and stand for 5 min under external magnetic field. Afterwards, the liquid supernatant was detected by UV-vis spectrophotometer. The adsorption capacity (Q mg g^{-1}) of MMIPs or MNIPs was calculated according to the following formula:

$$Q = \frac{(C_0 - C_t)V}{\mathrm{m}}$$

Where C_0 and C_t are the initial and final concentrations of HRP, s (mL) is the initial volume of HRP solution and m (mg) is the mass of dried MMIPs or MNIPs. Additionally, in order to evaluate the selectivity of MMIPs or MNIPs, imprinting factor (IF) was calculated according to the following formula:

$$IF = \frac{Q_{MMIPs}}{Q_{MNIPs}}$$

Adsorption kinetics study of MMIPs

The adsorption kinetics of the materials was studied by adding MMIPs or MNIPs into 0.4 mg mL^{-1} of HRP solution prepared in PB (pH 8.5, 200 mM). The above mixture was incubated at diverse time intervals ranging from 10 min to 90 min at 25 °C, and then was allowed to stand for 5 min under external magnetic field. After that, the liquid supernatant was measured by UV-vis spectrophotometer.

Specific adsorption study of MMIPs

To investigate the specific adsorption capability of Fe_3O_4@SiO_2-FPBA NPs, MMIPs and MNIPs, specific adsorption experiments were carried out. The aforementioned materials were respectively added into the mixed solution of BSA, OVA and HRP which were prepared in PB (pH 8.5, 200 mM) at a concentration of 0.4 mg mL^{-1}. After incubation at 25 °C for 40 min, the mixture stood for 5 min under external magnetic field. And then the liquid supernatant was measured by UV-vis spectrophotometer.

Real sample analysis of MMIPs

A 20-fold-diluted fetal bovine serum (FBS) in PB (pH 7.4, 200 mM) was spiked with HRP to prepare 0.2 mg mL^{-1} HRP solution. 8 mg of MMIPs were added into 6 mL of the above solution, incubating for 40 min under room temperature. After the supernatant and MMIPs were separated with an external magnet, the supernatant was measured with UV-Vis spectrophotometer [31].

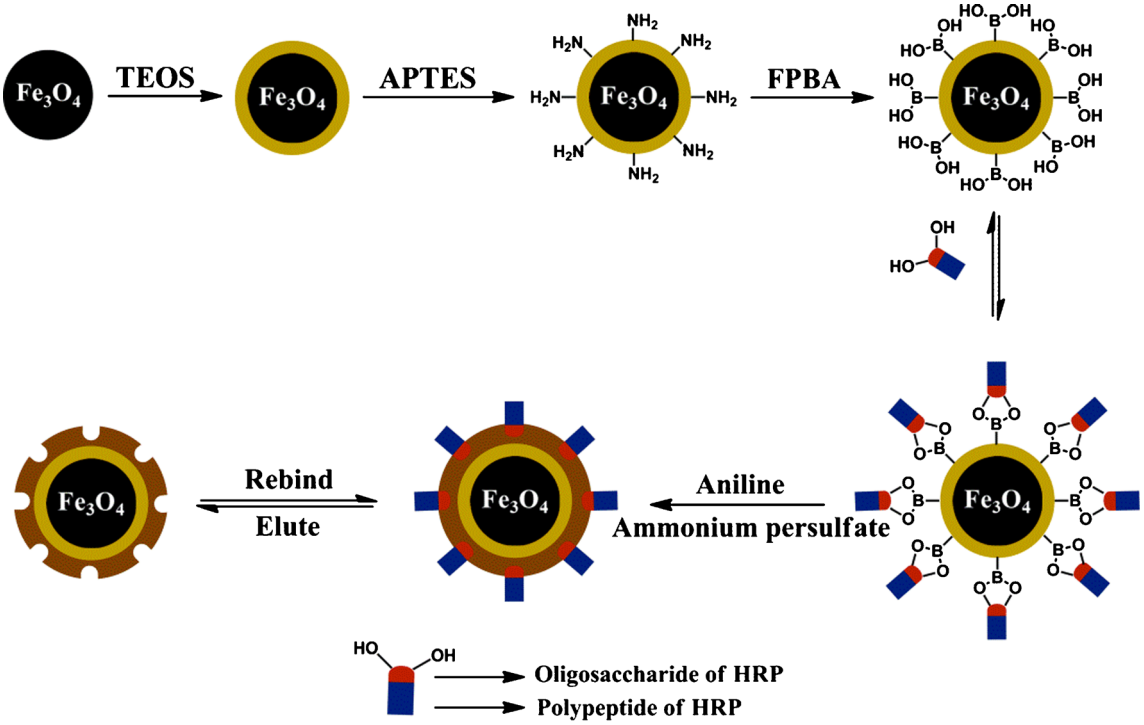

Fig. 1 Schematic of the prepared procedure of MMIPs

Results and discussion

Characterization

The structure of Fe_3O_4 NPs, Fe_3O_4@SiO_2 NPs, Fe_3O_4@SiO_2-APTES NPs, Fe_3O_4@SiO_2-FPBA NPs and MMIPs were separately analyzed by FT-IR (Fig. S1). The sharp peak at 580 cm^{-1} (curves a-e) assigned to the stretch of Fe-O vibration gradually become weak (curves band e) for the sake of forming shell on the surface of Fe_3O_4 NPs. Comparing with the infrared spectrum of Fe_3O_4 NPs, a sharp peak of Si-O-Si group vibration appears at 1100 cm^{-1} (curves b-e), indicating the successful wrapping of SiO_2 on the surface of Fe_3O_4 NPs. Characteristics peaks at 2948 cm^{-1} and 2920 cm^{-1} (curves c-e) attributed to the stretch of methylene vibration arise comparing with the infrared data of Fe_3O_4@SiO_2 NPs, showing APTES was grafted on the Fe_3O_4@SiO_2 NPs successfully. In comparison to curve c, a shoulder peak at 1420 cm^{-1} and 1376 cm^{-1} (curves d and e) resulted from B-O adsorption emerge, proving that FPBA had been anchored on the surface of nanoparticles. In curve e, the appearance of characteristics peaks of C = C stretching vibration of benzene ring at 1577 cm^{-1} and 1512 cm^{-1} indicate a shell of polyaniline was successfully formed on the surface of nanoparticles.

In order to identify the chemical compositions of Fe_3O_4@SiO_2-APTES NPs and Fe_3O_4@SiO_2-FPBA NPs, X-ray photoelectron spectroscopy (XPS) analysis was carried out. As observed from Fig. S2a, the XPS spectrum of Fe_3O_4@SiO_2-APTES NPs in which the peaks at 101, 285, 401, 534 and 712 eV is assigned to Si2p, C1s, N1 s, O1s and Fe2p, obviously confirm the existence of Si, C, N, O and Fe on the Fe_3O_4@SiO_2-APTES NPs. Inspected from Fig. S2b, besides the above peaks, the B1s peak around 186 eV is also observed which obviously reveals that FPBA as functional monomer had been successfully grafted on the surface of nanoparticles.

The morphologies of Fe_3O_4 NPs, Fe_3O_4@SiO_2 NPs, MMIPs and MNIPs were characterized by TEM images. The TEM displays that well-dispersed and uniform sphere-shaped Fe_3O_4 NPs with diameter about 200 nm (Fig. 2a) were prepared. The TEM image of Fe_3O_4@SiO_2 NPs (Fig. 2b) exhibits that Fe_3O_4 NPs are coated with SiO_2 uniformly. Additionally, the core-shelled Fe_3O_4@SiO_2 NPs still display good dispersity. After the formation of polymerized imprinted shell, the MMIPs (Fig. 2c) and MNIPs (Fig. 2d) do not appear sensible aggregation which is favorable for eluting and rebinding templates. Moreover, the TEM images of MMIPs prepared under different polymerization time intervals were also carried out. Fig. 3 shows that the imprinted layer of polyaniline increasing and the reduced dispersity of MMIPs follow with the extended polymerization time. The dynamic light scattering (DLS) was applied to test averaged hydrodynamic diameters of the Fe_3O_4 NPs, Fe_3O_4@SiO_2 NPs, MMIPs and MNIPs and their averaged diameters are 303 ± 12 nm, 360 ± 13 nm, 382 ± 18 nm and 391 ± 14 nm, respectively. The results (Fig. 2e-h) show that the prepared materials with homogeneous particles size. According

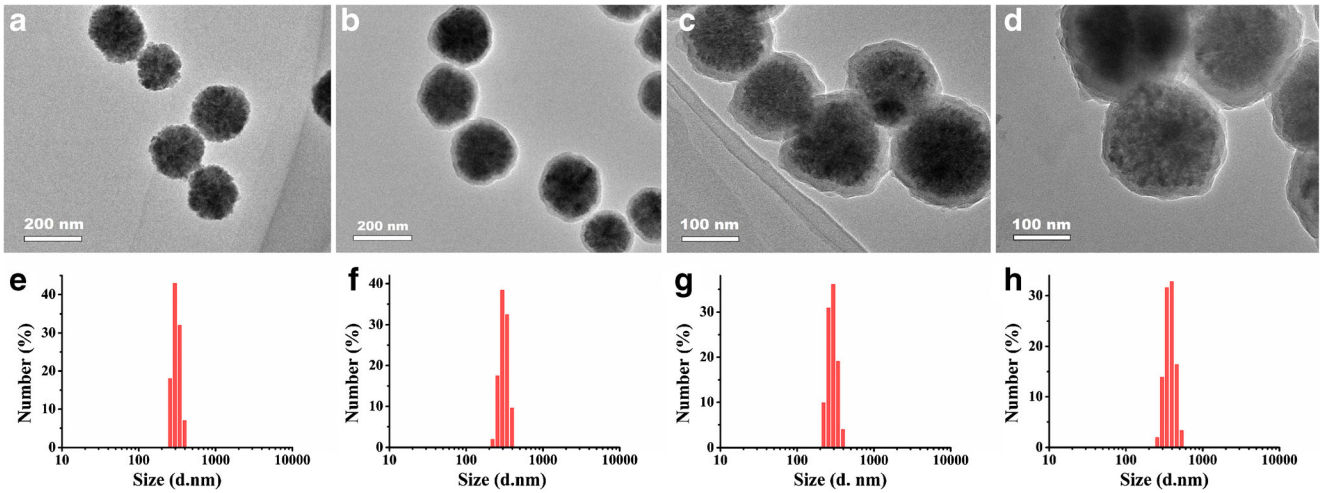

Fig. 2 TEM image and DLS size distribution graphs of (**a** and **e**) Fe_3O_4 NPs, (**b** and **f**) Fe_3O_4@SiO_2 NPs, (**c** and **g**) MMIPs, and (**d** and **h**) MNIPs

to the DLS, the averaged thickness of the imprinted layer is about 10 nm.

The VSM results of Fe_3O_4 NPs, Fe_3O_4@SiO_2 NPs and MMIPs (Fig. S3) detected at room temperature, no hysteresis is observed. Both remanence and coercivity are zero, indicating the superparamagnetism of the nanoparticles. Inspected from curves Fig. S3b and c, the slightly decreased saturated magnetic value is attributed to the existence of imprinted polymerized layer, which also confirms a rather thin imprinted polymerized layer generated.

Effect of imprinted layer thickness on the adsorption properties of MMIPs

Well dispersity is a sufficient condition for MMIPs to have excellent adsorption property since well dispersity enables more adsorption sites on MMIPs to be exposed. However, conventional MMIPs ordinarily are coated with thick imprinted layers which tend to wrap many nanoparticles together, leading to concealed adsorption sites and the incomplete templates eluting. For these reasons, it is practical to prepare MMIPs with thin imprinted layer to improve the dispersity of MMIPs. The thickness of imprinted layer is intimately associated with polymerization time as can be seen in Fig. 3. Thus, diverse polymerized time from 10 min to 40 min was investigated to obtain the optimal thickness of imprinted layer. Fig. 3a shows that the imprinted layer is too thin which is unfavorable for the adsorption of MMIPs for HRP when the polymerized times are 10 min and 20 min. When the polymerized time reaches 30 min, satisfactory adsorption capacity and high imprinting factor is gained. However, when the polymerized time prolonged to 40 min, the adsorption properties are

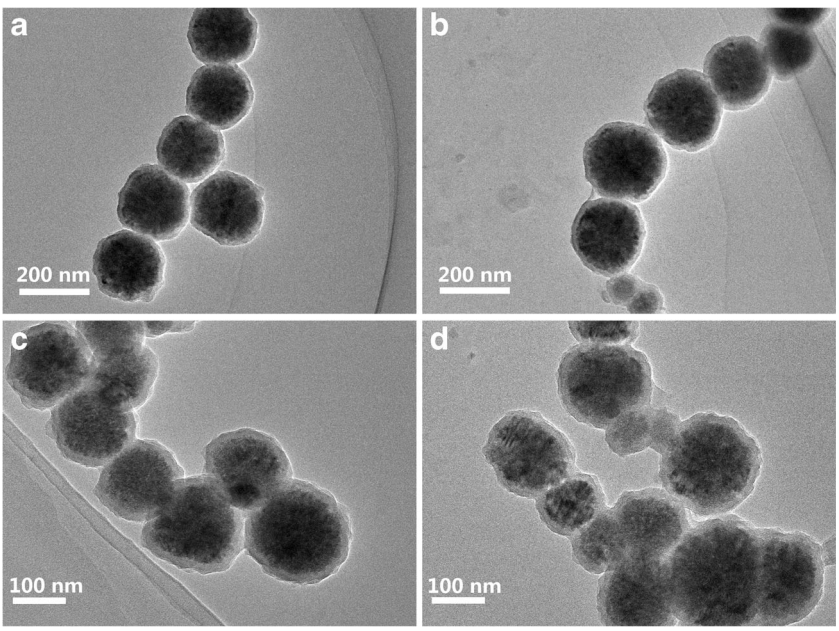

Fig. 3 TEM images of MMIPs prepared under different polymerization time intervals **a** 10 min, **b** 20 min, **c** 30 min, and **d** 40 min

unsatisfied. The imprinted layer is too thick which causes unsatisfied adsorption capacities since more MMIPs tend to aggregate and binding sites are omitted. Thus, the thickness of the imprinted layers play an important role, thin polymer layers can reduce the embedment of HRP and accelerating mass transfer of the templates.

Effect of pH on the adsorption properties of MMIPs

In order to anchor HRP efficiently, six batch experiments with different pH (6.5, 7.5, 8.5, 9.5, 10.5) of PB within the realm of the favorable adsorption pH of FPBA for HRP were carried out [10]. Fig. 4b shows that from 8.5 to 6.5 of pH, the interaction between FPBA and HRP is reduced, therefor the adsorption capacity of the MMIPs exhibits decline trend. From 8.5 to 10.5, the adsorption capabilities of MMIPs toward HRP also tend to decrease owing to the activity of HRP is decreased gradually. Therefore, the value of 8.5 is chosen as the most proper pH.

Adsorption kinetics of MMIPs

The diffusion limitation which restricts the ease of templates adsorption and removal is one of the major difficulties faced by macromolecules for imprinting. Based on the above consideration, adsorption kinetics was also studied with the initial HRP solution (0.4 mg mL^{-1}). Fig. 5a shows that both MMIPs and MNIPs have fast adsorption kinetics. In the first 40 min, the adsorption capacity increases quickly and reached adsorption equilibrium subsequently. The fast mass transfer rate of HRP is related to the thin imprinted layer. To further realize the adsorption kinetics, the second-order kinetic model was used to analyze the kinetics data. The second-order kinetic model is shown as follows:

$$\frac{t}{Q_t} = \frac{1}{K_2 Q_e^2} + \frac{t}{Q_e} = \frac{1}{v_0} + \frac{t}{Q_e}$$

Where Q_t and Q_e are the amount of HRP adsorbed on MMIPs or MNIPs at the time t (min) and equilibrium, separately. v_0 is the initial adsorption rate of MMIPs or MNIPs.

The relatively high correlation coefficients ($r > 0.99$) in Table 1 indicates that the second-order kinetic model suits to characterize adsorption kinetics. As a result, the rate-limiting step of adsorption kinetics is chemical adsorption. [32]

Adsorption isotherms of MMIPs

In order to investigate the maximum adsorption capacity of MMIPs toward HRP, adsorption isothermal was carried out with different initial HRP concentration ranging from 0 to 0.5 mg mL^{-1}. Below the concentration of 0.4 mg mL^{-1} in Fig. 5c, the adsorption capacity increases greatly along with the increased concentration of HRP. The great gap of adsorption capacity between MMIPs and MNIPs indicates the imprinted cavities are formed on the surface of MMIPs. In order to further learn about isothermal adsorption, Langmuir model is applied to describe the data of adsorption isotherms, which is expressed as follows:

$$\frac{C_e}{Q_e} = \frac{C_e}{Q_m} + \frac{1}{k_d Q_m}$$

Where C_e (mg mL^{-1}) is the concentration of HRP at equilibrium, Q_e (mg g^{-1}) and Q_m (mg g^{-1}) are the experimental and theoretical adsorption capacity of MMIPs or MNIPs for HRP, respectively and k_d (mL mg^{-1}) is the Langmuir adsorption equilibrium constant related to the affinity of MMIPs or MNIPs for HRP [36].

Inspected from Table 1, the high correlation coefficient ($r > 0.99$) confirms that the data of adsorption isothermal fitted the Langmuir model well. The maximum adsorption capacity (61.98 mg g^{-1}) obtained from experiment is close to the theoretical adsorption capacity (67.52 mg g^{-1}). Therefore, the adsorption of MMIPs toward HRP can be monolayer adsorption. [32]

Specific recognition capability of MMIPs

Glycoprotein OVA (Mw 45 kDa, pI 4.7) and non-glycoprotein BSA (Mw 66 kDa, pI 4.8) were selected as the interferences to investigate the specific recognition ability of MMIPs towards

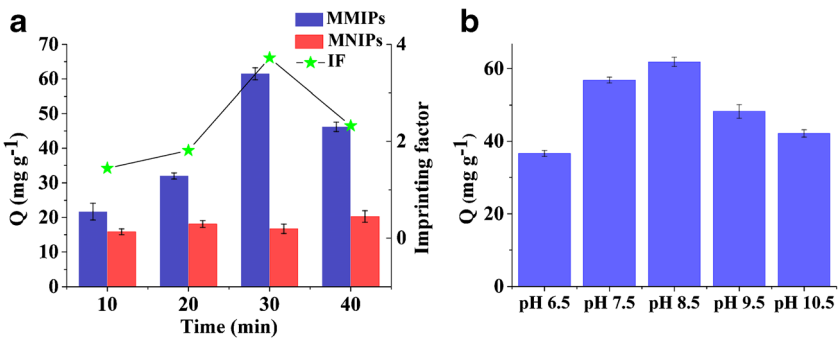

Fig. 4 The effect of **a** polymerization time and **b** reaction pH on the adsorption performance of MMIPs

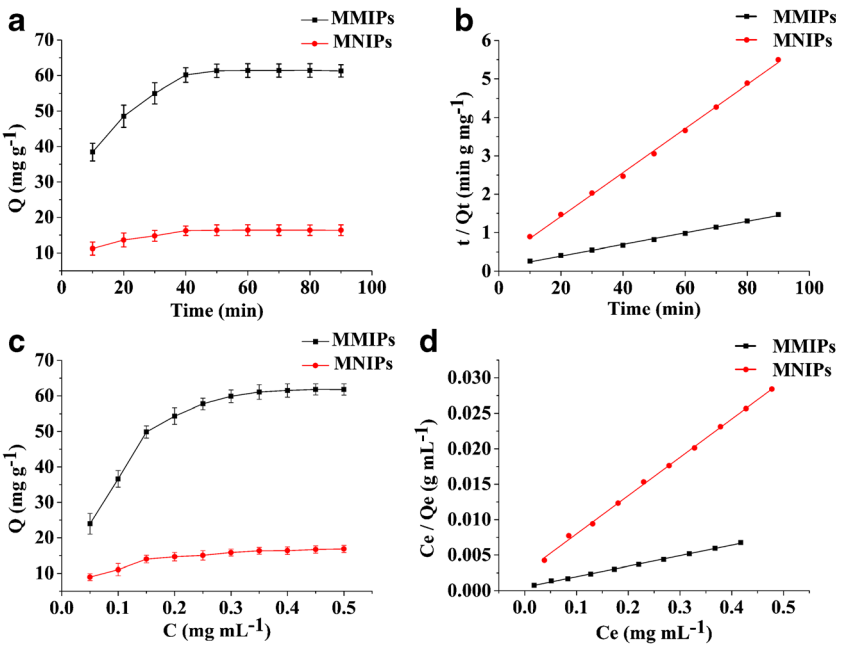

Fig. 5 Adsorption kinetics of MMIPs and MNIPs; **b** second-order kinetics model and **d** Langmuir model fit of HRP on MMIPs and MNIPs; **c** adsorption isothermal of MMIPs and MNIPs. V = 6 mL, m = 8 mg, PB (pH 8.5, 200 mM)

HRP (Mw 40 kDa, pI 7.2). The experiment was carried out by separately adding Fe_3O_4@SiO_2-FPBA, MMIPs and MNIPs into the protein mixture at concentration of 0.4 mg mL^{-1}, respectively. The rebinding condition is displayed in Fig. 6. The Fe_3O_4@SiO_2-FPBA NPs display the highest adsorption capacity for all proteins as boracic acids and remained amino groups interact with them. However, for glycoproteins of HRP and OVA, the absent imprinted layer inclined Fe_3O_4@SiO_2-FPBA NPs have no specific recognition ability toward HRP. Moreover, the Fe_3O_4@SiO_2-FPBA NPs tend to absorb more OVA since OVA contain much more glyco content than HRP. While for MMIPs, the great distinction of adsorption capacity between HRP and OVA informs that imprinted layer play a key role in specific recognition. Moreover, the lowest adsorption capacity was obtained for MNIPs toward all proteins, which further proved that imprinted cavities do not exist on the surface of MNIPs.

Reusability of the MMIPs

Reusability is one of the most important factors for the practical application of MIPs. The reusability of MMIPs was studied by using the same batch of MMIPs and MNIPs for continuous adsorption-desorption cycles shown in Fig. S4. After the eight cycles, for MMIPs, there is only a slight reduction of adsorption capacity from 61.98 to 55.41 mg g^{-1}, which can be ascribed to the part destruction of imprinted cavities. While for MNIPs, the adsorption capacity keeps almost constant after five continuous cycles since MNIPs have no specific binding sites for HRP.

Real sample analysis

In order to investigate the practicability of MMIPs, the prepared MMIPs were applied to extract HRP from FBS. Fig. 7

Table 1 Equations and parameters of adsorption kinetics and isothermal of MMIPs and MNIPs

Model	Parameters	MMIPs	MNIPs
Second-order kinetics	Equation	$t/Q_t = 0.01501\ t + 0.0924$	$t/Q_t = 0.05727\ t + 0.27392$
	Q_e (mg g^{-1})	66.62 mg g^{-1}	17.46 mg g^{-1}
	K_2 (g mg^{-1} min^{-1})	0.002438 g mg^{-1} min^{-1}	0.01198 g mg^{-1} min^{-1}
	v_0 (mg g^{-1} min^{-1})	10.82 mg g^{-1} min^{-1}	3.651 mg g^{-1} min^{-1}
	r	0.9988	0.9992
Langmuir isothermal	Equation	$C_e/Q_e = 0.0148\ C_e + 0.00048$	$C_e/Q_e = 0.0508\ C_e + 0.00257$
	Q_e (mg g^{-1})	67.52 mg g^{-1}	18.49 mg g^{-1}
	k_d (mL mg^{-1})	30.61 mL mg^{-1}	21.04 mL mg^{-1}
	r	0.9994	0.9994

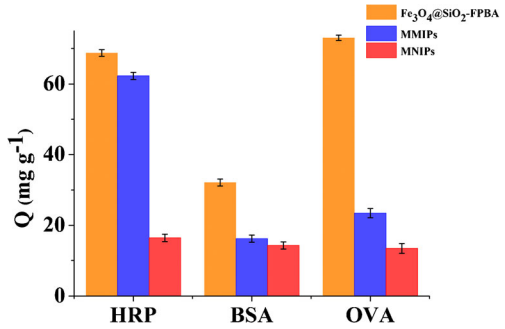

Fig. 6 The selectivity of MMIPs and MNIPs toward HRP

shows the UV-Vis spectrum of diluted FBS (a), 0.2 mg mL^{-1} HRP in diluted FBS after (b) and before (c) adsorbed by MMIPs. Inspected from Fig. 7a, the UV-Vis spectrum of diluted FBS showed a strong absorbance at 298 nm and a weak absorbance at 410 nm due to the adsorption of BSA and BHb, separately [30]. After HRP was added into the FBS, the adsorption peak shifted to 400 nm (Fig. 7c) which is the adsorption peak of HRP. Observed from Fig. 7b, apparently reduction of absorption at 400 nm appeared due to the extraction of MMIPs toward HRP. The result further confirmed that the MMIPs prepared by this way have excellent extraction capability.

Conclusion

This study provides a strategy to improve the dispersity of MMIPs by coating uniform silica on Fe_3O_4 NPs and precisely controlling the polymerization time of aniline. As a result, the number of adsorption sites on the MMIPs was increased and mass transfer route was reduced. Moreover, the introduction of FPBA as functional monomer also relieves the template adsorption and elution difficulty. Stemming from these reasons, the prepared MMIPs showed improved adsorption capacity, excellent selectivity and fast mass transfer rate toward HRP. Moreover, considering the trend in simultaneous determination of several tumor markers in clinical, improved MMIPs which could simultaneously selective extract several kinds of glycoproteins in a single run would be researched in future work.

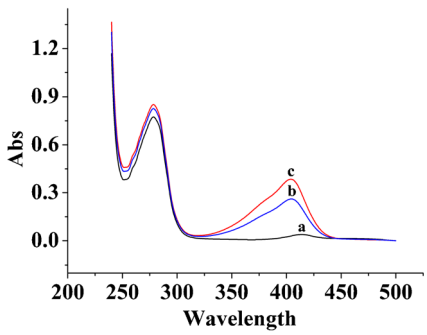

Fig. 7 UV-Vis spectrum of FBS diluted 20-fold **a**, 0.2 mg mL^{-1} HRP in diluted FBS after **b**, and before **c** absorbed with MMIPs

Acknowledgements Financial supports from the National Natural Science Foundation of China (No. 21475142, 21611140105), CAS President's International Fellowship Initiative (SL: 191), the funds for Distinguished Young Scientists of Gansu (1506RJDA281) and the top priority program of "One-Three-Five" Strategic Planning of Chinese Academy of Sciences are gratefully acknowledged.

Compliance with ethical standards The author(s) declare that they have no competing interests.

References

1. Arnal-Estapé A, Nguyen DX (2015) Sweets for a bitter end: lung cancer cell–surface protein glycosylation mediates metastatic colonization. Cancer Discov 5(2):109–111
2. Christiansen MN, Chik J, Lee L, Anugraham M, Abrahams JL, Packer NH (2014) Cell surface protein glycosylation in cancer. Proteomics 14(4–5):525–546
3. Schedin-Weiss S, Winblad B, Tjernberg LO (2014) The role of protein glycosylation in Alzheimer disease. FEBS J 281(1):46–62
4. Yang Q, Zhu Y, Luo B, Lan F, Wu Y, Gu ZW (2017) pH-responsive magnetic Nanospheres for reversibly selective capture and release of glycoproteins. J Mater Chem B 5(6):1236–1245
5. Tan L, Che K, Huang C, Peng RF, Luo XY, Yang R, Tang YF (2015) A fluorescent turn-on detection scheme for α-fetoprotein using quantum dots placed in a boronate-modified molecularly imprinted polymer with high affinity for glycoproteins. Microchim Acta 182(15–16):2615–2622
6. Zhang Y, Zhuang YT, Shen HY, Chen XW, Wang JH (2017) A super hydrophilic silsesquioxane-based composite for highly selective adsorption of glycoproteins. Microchim Acta 184(4):1037–1044
7. Zhu J, Wang FJ, Chen R, Cheng K, Xu B, Guo ZM, Liang XM, Ye ML, Zou HF (2012) Centrifugation assisted microreactor enables facile integration of trypsin digestion, hydrophilic interaction chromatography enrichment, and on-column deglycosylation for rapid and sensitive N-glycoproteome analysis. Anal Chem 84(11):5146–5153
8. Zhou YR, Aebersold R, Zhang H (2007) Isolation of N-linked Glycopeptides from plasma. Anal Chem 79(15):5826–5837
9. Li HJ, Wang HY, Liu YC, Liu Z (2012) A benzoboroxole-functionalized monolithic column for the selective enrichment and separation of cis-diol containing biomolecules. Chem Commun 48(34):4115–4117
10. Xue Y, Shi WJ, Zhu BJ, Gu X, Wang Y, Yan C (2015) Polyethyleneimine-grafted boronate affinity materials for selective enrichment of cis-diol-containing compounds. Talanta 140:1–9
11. Lin Z, Sun LX, Liu W, Xia ZW, Yang HH, Chen GN (2014) Synthesis of boronic acid-functionalized molecularly imprinted silica nanoparticles for glycoprotein recognition and enrichment. J Mater Chem B 2(6):637–643
12. Barahona F, Díaz-Álvarez M, Turiel E, Martín-Esteban A (2016) Molecularly imprinted polymer-coated hollow fiber membrane for the microextraction of triazines directly from environmental waters. J Chromatogr A 1442:12–18
13. Hu X, Xie LW, Guo JF, Li H, Jiang XY, Zhang YP, Shi SY (2015) Hydrophilic gallic acid–imprinted polymers over magnetic mesoporous silica microspheres with excellent molecular recognition ability in aqueous fruit juices. Food Chem 179:206–212

14. Nehme H, Nehme R, Lafite P, Routier S, Morin P (2012) New development in in-capillary electrophoresis techniques for kinetic and inhibition study of enzymes. Anal Chim Acta 722:127–135
15. Li HF, Xie T, Ye LL, Wang YW, Xie CG (2017) Core-shell magnetic molecularly imprinted polymer nanoparticles for the extraction of triazophos residues from vegetables. Microchim Acta 184: 1011–1019
16. Altuna S, Cakıroglu B, Özacar M, Özacar M (2015) A facile and effective immobilization of glucose oxidase on tannic acid modified $CoFe_2O_4$ magnetic nanoparticles. Colloids Surf B 136:963–970
17. Hou C, Qi ZG, Zhu H (2015) Preparation of core-shell magnetic polydopamine/alginate biocomposite for *Candida rugosa* lipase immobilization. Colloids Surf B 128:544–551
18. Li QR, Yang KG, Li SW, Liu LK, Zhang LH, Liang Z, Zhang YK (2016) Preparation of surface imprinted core-shell particles via a metal chelating strategy: specific recognition of porcine serum albumin. Microchim Acta 183:345–352
19. Hou C, Zhu H, Li YF, Li YJ, Wang XY, Zhu WW, Zhou RD (2015) Facile synthesis of oxidic PEG-modified magnetic polydopamine nanospheres for *Candida rugosa* lipase immobilization. Appl Microbiol Biotechnol 99(3):1249–1259
20. Niu M, Pham-Huy C, He H (2016) Core-shell nanoparticles coated with molecularly imprinted polymers: a review. Microchim Acta 183(10):2677–2695
21. Yin YQ, Xiao Y, Lin G, Xiao Q, Lin Z, Cai ZW (2015) An enzyme-inorganic hybrid nanoflower based immobilized enzyme reactor with enhanced enzymatic activity. J Mater Chem B 3(11):2295–2300
22. Ma RT, Ha W, Chen J, Shi YP (2016) Highly dispersed magnetic molecularly imprinted nanoparticles with well-defined thin film for the selective extraction of glycoprotein. J Mater Chem B 4(15): 2620–2627
23. Royvaran M, Taheri-Kafrani A, Isfahani AL, Mohammadi S (2016) Functionalized superparamagnetic graphene oxide nanosheet in enzyme engineering: a highly dispersive, stable and robust biocatalyst. Chem Eng J 288:414–422
24. Unsoy G, Yalcin S, Khodadust R, Gunduz G, Gunduz U (2012) Synthesis optimization and characterization of chitosan-coated iron oxide nanoparticles produced for biomedical applications. J Nanopart Res 14(11):1–13
25. Betancor L, López-Gallego F, Hidalgo A, Alonso-Morales N, Mateo GDOC, Fernández-Lafuente R, Guisán JM (2006) Different mechanisms of protein immobilization on glutaraldehyde activated supports: effect of support activation and immobilization conditions. Enzyme Microb Technol 39(4):877–882
26. Deng H, Li X, Peng Q, Wang X, Chen J, Li Y (2005) Monodisperse magnetic single-crystal ferrite microspheres. Angew Chem 117(18):2842–2845
27. Pan C, Hu B, Li W, Sun Y, Ye H, Zeng X (2009) Novel and efficient method for immobilization and stabilization of β-d-galactosidase by covalent attachment onto magnetic Fe_3O_4-chitosan nanoparticles. J Mol Catal B 61(3):208–215
28. Shao MF, Ning FY, Zhao JW, Wei M, Evans DG, Duan X (2012) Preparation of Fe_3O_4@SiO_2@layered double hydroxide Core–Shell microspheres for magnetic separation of proteins. J Am Chem Soc 134(2):1071–1077
29. Yang S, Zhang X, Zhao WT, Sun LQ, Luo AQ (2016) Preparation and evaluation of Fe_3O_4 nanoparticles incorporated molecularly imprinted polymers for protein separation. J Mater Sci 51(2):937–949
30. Li YX, Chen YT, Huang L, Lou BY, Chen GN (2017) Creating BHb-imprinted magnetic nanoparticles with multiple binding sites. Analyst 142:302–309
31. Zhang W, Liu W, Li P, Xiao HB, Wang H, Tang B (2014) A fluorescence nanosensor for glycoproteins with activity based on the molecularly imprinted spatial structure of the target and boronate affinity. Angew Chem 126(46):12697–12701
32. Gao RX, Mu XR, Hao Y, Zhang LL, Zhang JJ, Tang YH (2014) Combination of surface imprinting and immobilized template techniques for preparation of core–shell molecularly imprinted polymers based on directly amino-modified Fe_3O_4 nanoparticles for specific recognition of bovine hemoglobin. J Mater Chem B 2(12):1733–1741